Observation of Plasma Wake-Field Effects during High-Current Relativistic Electron-Beam Transport

Joel D. Miller, Ralph F. Schneider, Daniel J. Weidman,[a] and Han S. Uhm
Naval Surface Warfare Center, Silver Spring, Maryland 20903-5000

Khanh T. Nguyen
Mission Research Corporation, Newington, Virginia 22122
(Received 25 June 1991)

Modulation of the beam current has been observed during ion-focused-regime (IFR) transport of a high-power relativistic electron beam propagating through a low-density background plasma. In this experiment, a 1.7-MeV, 1-kA rise-time-sharpened electron beam is transported in a KrF-excimer-laser-produced IFR channel in trimethylamine gas. The IFR channel is immersed in a low-density plasma-filled transport tube. We present experimental measurements and computer simulations demonstrating modulation of this high-current relativistic electron beam near the low-density background plasma frequency.

PACS numbers: 41.80.Ee, 52.40.Mj

Plasma wake fields are well known in the high-energy physics community. The plasma-wake-field accelerator (PWFA) [1] utilizes the longitudinal electric fields in plasma waves excited by a short-duration bunched relativistic electron beam as a source of high accelerating gradients. In the PWFA, intense electron bunches are utilized as a driver beam to excite wake fields in a high-density plasma. These wake fields are then used to accelerate a low-current trailing beam [2–4]. The work reported here involves experimental measurements on high-current (kA level) relativistic electron beams whose transport is strongly influenced by self-induced wake fields.

A high-current relativistic electron beam injected into a preionized plasma channel causes channel electrons to be expelled by the electrostatic force generated by the head of the beam and permits stable electron-beam transport [5–9]. If the plasma channel is immersed in a low-density background plasma, both channel electrons and plasma electrons inside the charge neutralization radius are ejected by the beam head, provided the combined channel and background plasma density is less than the beam density. The charge neutralization radius is the point at which the total enclosed channel and background plasma ion charge is equal to the beam charge. For uniform beam, channel, and plasma density profiles, the charge neutralization radius can easily be shown to be

$$r_n = r_b \left[\left(\frac{r_c}{r_b} \right)^2 + \frac{1-(r_c/r_b)^2 f_e}{g} \right]^{1/2},$$

where r_b is the beam radius, r_c is the channel radius, $f_e = n_i/n_b$ is the space-charge neutralization fraction and is the ratio of the channel ion density to the electron-beam density, and $g = n_p/n_b$ is the ratio of the ion density outside the channel to the electron-beam density. The background electrons beyond the charge neutralization radius are not expelled, but they are perturbed by the beam head and begin to oscillate at a frequency near that of the electron plasma frequency of the low-density background plasma, $\omega_p = (n_p e^2/\epsilon_0 m_e)^{1/2}$. These radial plasma oscillations produce an electrostatic wake field with electric-field components in the radial and axial directions. The longitudinal component of this field, traveling with the beam, causes accelerating and decelerating forces on beam electrons leading to beam energy and current modulation. These effects were first observed for high-current beams in computer simulations [10] and were seen to lead to eventual beam disruption. Most of what is known about this beam-plasma interaction is due to analytical calculations [11,12] and numerical simulations [10–12] with no direct experimental measurements.

In the experiment, a 1.7-MeV, 6-kA, 30-ns electron beam produced by a Febetron 705 is passed through a beam rise-time sharpener and matched onto a laser-produced IFR channel in trimethylamine (TMA) gas. Figure 1 is a schematic diagram of the experiment. The electron beam is generated from a 2.5-cm-diam velvet cathode and is extracted into a beam rise-time-sharpening cell through a 6-μm aluminized Mylar anode foil. The rise-time-sharpener cell [13] uses a single magnetic lens to preferentially focus the high-energy portion of the beam at an aperture. This results in a 1-kA electron beam, with a 5-ns rise time and a 13-ns flattop, exiting the rise-time-sharpening cell through a second aluminized Mylar foil in front of the 3-cm-diam graphite aperture plate. The beam extracted through this aperture is matched onto a KrF-excimer-laser–ionized IFR channel.

The 3-cm-diam-laser–ionized channel is formed by two-step photoionization of TMA using a 750-mJ, 248-nm, 30-ns KrF excimer laser. The TMA gas flows through the transport chamber continuously to provide a stable gas pressure in the range 0.2–0.8 mTorr. These TMA pressures result in space-charge neutralization fractions sufficient to efficiently propagate the electron beam in the absence of a background plasma. The beam

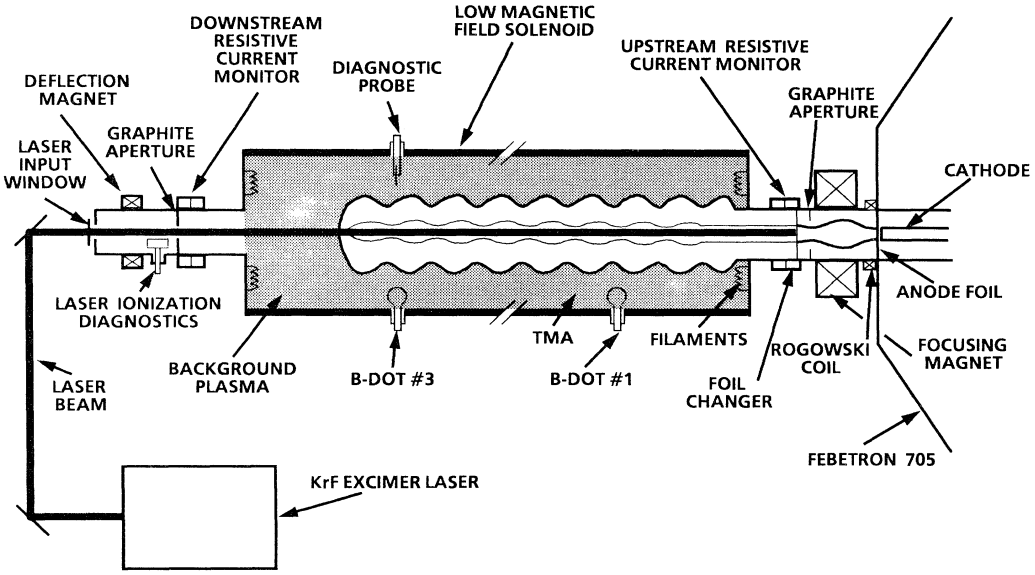

FIG. 1. Schematic of the plasma-wake-field experiment.

rise-time-sharpener cell and the diode region are maintained at a lower pressure, on the order of 10^{-5} Torr, to prevent diode-shorting or gas-focusing effects. The TMA pressure is measured with ionization gauges calibrated to a Baratron capacitance manometer. The laser is fired to ionize the TMA typically 500 ns before the voltage is applied to the diode.

The laser-produced channel is centered in a 0.5-m-diam, 3.6-m-long plasma-filled transport chamber. The low-density background plasma filling the transport chamber is generated by a hot-filament discharge in the low-pressure TMA gas. The discharge is pulsed for durations less than 1 ms to reduce the level of TMA fragmentation before the laser is fired [14]. The gas pressure is sufficiently low that beam-induced ionization of the TMA is negligible. Plasma characteristics measured by Langmuir [15] and microwave resonator [16] probe techniques indicate that the plasma has good uniformity axially, radially, and azimuthally [17]. A low axial magnetic field (on the order of 5 G) is present for plasma confinement and to improve the uniformity. This field is sufficiently small so as not to influence the electron-beam dynamics. The plasma density is adjustable in the range 10^8 to 5×10^9 cm^{-3}.

The beam current is monitored prior to injection into the plasma-filled transport chamber and after exciting the chamber by resistive wall current monitors [18]. Uncalibrated, single-turn B-dot loops [19] located axially along the transport chamber monitor the evolution of the modulation of the current. Diametrically opposing B-dot loops could also be configured to detect transverse beam centroid motion [19]. It should be noted that both monitors are sensitive to the net current flowing in the transport chamber. A scintillator photodiode observed the x-ray signal emitted when the beam electrons were deflected to the wall at the end of the transport chamber to avoid striking the laser input window.

Initial experimental measurements have demonstrated very well-defined current oscillations impressed upon the electron beam after traversing the 3.6-m-long transport chamber. These oscillations are in the range 150–300 MHz and are very close to the electron plasma frequency of the low-density background plasma. In the absence of the background plasma, the most efficient electron-beam transport occurred for a space-charge neutralization fraction of $f_e \approx 0.9$ as determined by the laser channel ionization measurements. This is indicative of a fairly high transverse beam temperature and is common to electron beams generated and propagated using these techniques.

The evolution of the current oscillations is characterized in the typical wave forms shown in Fig. 2. Figure 2(a) shows the response of the resistive wall current monitors in the absence of the background plasma. The currents are shown prior to the entrance of the beam into the transport chamber (upper wave form) and after exiting from the chamber (lower wave form). Examination of the transported current wave form indicates a steepening of the current rise time with an associated spike at the front end of the pulse. This is due to a combination of inductive beam erosion and the fact that the beam voltage pulse is nearly sinusoidal and varies throughout the current pulse [20]. Figures 2(b)–2(d) illustrate the development of current oscillations with increasing background plasma density. The plasma densities have been inferred from dc-biased (+40 V) Langmuir probe data without any correction for finite sheath effects. The

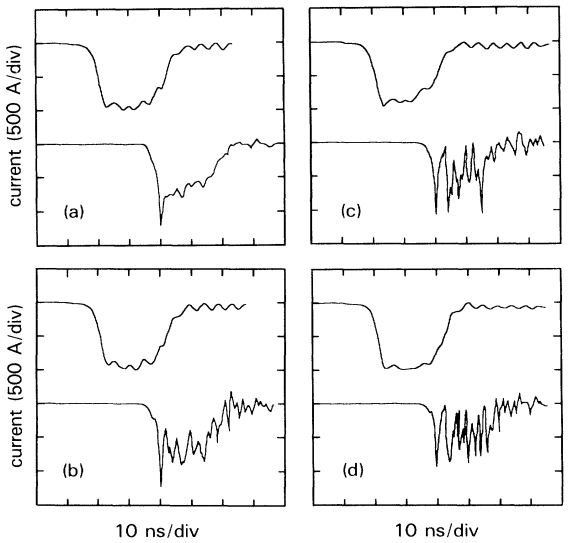

FIG. 2. Current wave forms from the resistive wall current monitors; (a) $n_p=0$, (b) $n_p=1.0\times10^9$ cm^{-3}, (c) $n_p=1.5\times10^9$ cm^{-3}, (d) $n_p=2.0\times10^9$ cm^{-3}. Top (bottom) wave form: current entering (exiting) the transport chamber.

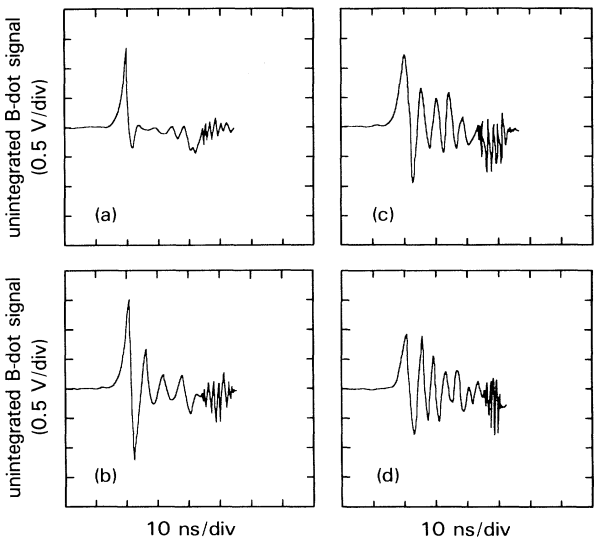

FIG. 3. Unintegrated B-dot-loop response 0.9 m downstream from the entrance to the plasma-filled transport chamber: (a) $n_p=0$, (b) $n_p=6.3\times10^8$ cm^{-3}, (c) $n_p=1.0\times10^9$ cm^{-3}, and (d) $n_p=1.5\times10^9$ cm^{-3}.

space-charge neutralization fraction at the peak beam current for all the data presented here was $f_e\approx0.9$, giving a neutralization radius r_n ranging from 3.0 cm [Fig. 2(b)] to 2.4 cm [Fig. 2(d)]. For these experimental parameters, g assumes values in the range $0\leq g\leq0.06$, indicating that the low-density background plasma does not contribute significantly to the space-charge neutralization fraction of the channel. The data in Figs. 2(c) and 2(d) indicate that the current becomes severely modulated after only 3.6 m of transport in the plasma background. Measurements performed with the resistive wall current monitors and the B-dot loop configured to detect transverse beam motion observed no discernible indication of beam motion transverse to the direction of propagation. Increasing the plasma density higher than that shown in Fig. 2(d) resulted in loss of transport efficiency and eventual beam disruption as indicated by the current monitors and the x-ray signal picked up by the scintillator photodiode.

The frequency of oscillation is more readily determined from the unintegrated B-dot-loop data. Figure 3 shows the unintegrated B-dot-loop response from the probe located 0.9 m downstream from the entrance to the plasma-filled transport chamber. The current oscillations are quite clear and indicate an increasing frequency with increasing plasma density. The dependence of the background plasma density on the oscillation frequency obtained from the unintegrated B-dot-loop data is shown in Fig. 4. The solid line represents a least-squares fit of the data to a $n_p^{1/2}$ dependence. This functional dependence indicates that the experimentally observed current oscillation frequency scales quite well with the low-density background electron plasma frequency.

Numerical simulations have also been performed to predict the behavior of the electron beam in the plasma-filled chamber using the fully electromagnetic $2\frac{1}{2}$-dimensional particle-in-cell code MAGIC [21]. The beam and channel properties in the simulation correspond quite closely to the experimental conditions described previously. The transport chamber was filled with a uniform diffuse plasma at a density of 2×10^9 cm^{-3}. The evolution of the electron-beam current in the transport chamber at different axial locations is shown in Figs. 5(a)–5(d). The beam-current profile in Fig. 5(a) corresponds to the experimentally measured electron-beam current prior to injection to the plasma-filled chamber

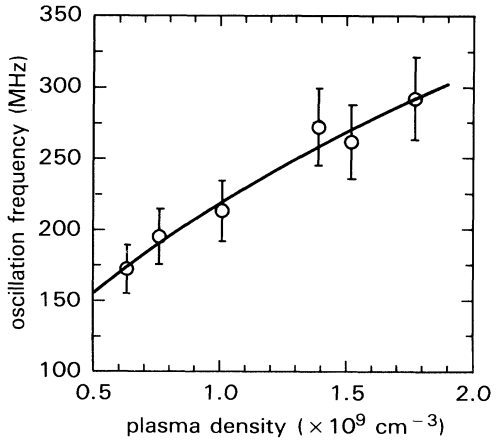

FIG. 4. Oscillation frequency from the unintegrated B-dot-loop data as a function of the background plasma density.

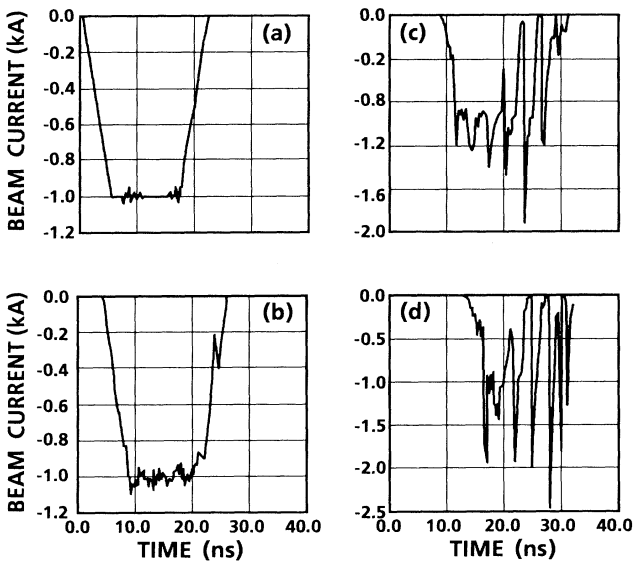

FIG. 5. Beam-current wave forms from the MAGIC simulation at (a) $z=0$ m, (b) $z=1.1$ m, (c) $z=2.3$ m, and (d) $z=3.4$ m downstream from the entrance to the plasma-filled transport chamber for $n_p=2.0\times10^9$ cm^{-3}.

and the simulation wave form in Fig. 5(d) to the experimentally measured wave form upon exiting from the chamber. The simulation clearly shows the ability of the diffuse plasma to strongly modulate the beam current. This result compares very well to the experimental data shown in Fig. 2.

We have observed very well-defined current oscillations impressed upon a high-current relativistic electron beam propagating in an IFR channel immersed in a low-density background plasma. Severe effects on beam-current transport have been observed for g parameter values in the range 0.03–0.06 after only 3.6 m of beam transport. Initial results indicate the frequency of current oscillation to be near the plasma frequency of the low-density background plasma, consistent with the predictions of plasma-wake-field theory and simulation.

The authors would like to thank J. Goldhar and W. C. Freeman for technical assistance, and G. Joyce for helpful discussions. This work was supported by the Strategic Defense Initiative Organization under funding document No. N0001490WX15505 and Independent Research funds at the Naval Surface Warfare Center.

[a]Permanent address: Advanced Technology and Research, Laurel, MD 20707.

[1] P. Chen, J. M. Dawson, R. W. Huff, and T. Katsouleas, Phys. Rev. Lett. **54**, 693 (1985).
[2] R. D. Ruth, A. W. Chao, P. L. Morton, and P. B. Wilson, Part. Accel. **17**, 171 (1985).
[3] J. B. Rosenzweig, P. Schoessow, B. Cole, W. Gai, R. Konecny, J. Norem, and J. Simpson, Phys. Rev. A **39**, 1586 (1989).
[4] J. B. Rosenzweig, D. B. Cline, B. Cole, H. Figueroa, W. Gai, R. Konecny, J. Norem, P. Schoessow, and J. Simpson, Phys. Rev. Lett. **61**, 98 (1988).
[5] W. E. Martin, G. J. Caporaso, W. M. Fawley, D. Prosnitz, and A. G. Cole, Phys. Rev. Lett. **54**, 685 (1985); G. J. Caporaso, F. Rainer, W. E. Martin, D. S. Prono, and A. G. Cole, Phys. Rev. Lett. **57**, 1591 (1986).
[6] R. L. Carlson, S. W. Downey, and D. C. Moir, J. Appl. Phys. **61**, 12 (1986).
[7] C. A. Frost, S. L. Shope, R. B. Miller, G. T. Leifeste, C. E. Crist, and W. W. Reinstra, IEEE Trans. Nucl. Sci. **32**, 2754 (1985).
[8] H. L. Buchanan, Phys. Fluids **30**, 231 (1987).
[9] S. L. Shope, C. A. Frost, G. T. Leifeste, and J. W. Poukey, Phys. Rev. Lett. **58**, 531 (1987).
[10] M. A. Mostrom and B. S. Newberger, Bull. Am. Phys. Soc. **31**, 1399 (1986).
[11] H. S. Uhm, Phys. Lett. A **149**, 469 (1990).
[12] H. S. Uhm and G. Joyce, Phys. Fluids B **3**, 1587 (1991).
[13] J. D. Miller, R. F. Schneider, H. S. Uhm, K. T. Nguyen, K. W. Struve, and D. J. Weidman, Naval Surface Warfare Center Technical Report No. NAVSWC TR 90-268, 1990 (unpublished).
[14] J. D. Miller, R. F. Schneider, and J. Goldhar, Naval Surface Warfare Center Technical Note No. NAVSWC TN90-326, 1990 (unpublished).
[15] F. F. Chen, in *Plasma Diagnostics Techniques,* edited by R. H. Huddlestone and S. L. Leonard (Academic, New York, 1965), p. 113.
[16] R. L. Stenzel, Rev. Sci. Instrum. **47**, 603 (1976).
[17] J. D. Miller, R. F. Schneider, H. S. Uhm, and D. J. Weidman, Naval Surface Warfare Center Technical Note No. NAVSWC TN 90-428, 1990 (unpublished); H. S. Uhm, J. D. Miller, R. F. Schneider, and D. J. Weidman, IEEE Trans. Plasma Sci. **19**, 535 (1991).
[18] K. W. Struve, in *Conference Record of the Workshop on Measurements of Electrical Quantities in Pulse Power Systems II* (IEEE, New York, 1988), Catalog No. 86CH2327-5, p. 36.
[19] S. Humphries, Jr., *Principles of Charged Particle Acceleration* (Wiley, New York, 1986), p. 278.
[20] J. R. Smith (private communication).
[21] B. Goplen, L. Ludeking, J. McDonald, G. Warren, and R. Worl, Mission Research Corporation Report No. MRC/WDC-R-216, 1989 (unpublished).